Forced oscillations dynamic tribometer with real-time insights of lubricated interfaces

M. Yahiaoui, E. Rigaud, D. Mazuyer, and J. Cayer-Barrioz
Laboratoire de Tribologie et Dynamique des Systèmes—UMR 5513 CNRS, École Centrale de Lyon, 69130 Écully, France

This paper presents an innovative forced oscillations dynamic tribometer, the CHRONOS tribometer, with a lubricated ball-on-flat contact configuration fitted out with an *in situ* optical visualization system and a triggered high-speed camera. The CHRONOS tribometer generates controlled oscillating kinematics by means of a shaker with a range of strokes from 5 μm to 2.5 mm and an oscillation frequency which can be adjusted from 5 Hz to 250 Hz. Displacement and velocity are measured using a vibrometer. The ball-on-flat mean contact pressure is set between 200 MPa and 600 MPa. During motion, the instantaneous normal and friction forces and the interfacial film thickness distribution (in the nanometer scale) are simultaneously measured. In addition to this instantaneous approach, a more macroscopic approach is developed in terms of moving averages of friction and velocity. Another parameter, the friction-velocity tilt angle, is also introduced. This last parameter may give information on the friction-velocity dependence. Eventually, the experiments performed on the CHRONOS device lead to the representation of synchronized temporal signals of displacement/velocity, friction, and lubricant central film thickness. This superimposition of key parameters reveals time effects introduced by the periodical fluid squeeze and flow in the contact. *Published by AIP Publishing.* [http://dx.doi.org/10.1063/1.4977234]

NOMENCLATURE

θ	=	friction-velocity cycles tilt angle, deg.
μ	=	friction coefficient
$\prod$	=	rectangular function.
E	=	Young modulus, Pa
E_d	=	dissipated energy, J
f	=	oscillation frequency, Hz
f_{max}	=	maximum frequency, Hz
f_T	=	transverse friction force, N
h	=	lubricant film thickness on a profile, m
h_c	=	lubricant central film thickness, m
k	=	natural integer
N_c	=	number of cycles
R	=	Hertz radius, m
R_a	=	surface roughness, m
t	=	time, s
T	=	signal period, s
x	=	displacement, m
$\dot{x}$	=	velocity, m/s
$\dot{x}_{max}$	=	maximum velocity, m/s

I. INTRODUCTION

Many sliding contacts in industrial and biological applications are subjected to transient kinematics (e.g., piston rings/cylinder contacts, knee) or simply intermittent operating conditions (e.g., start and stop). However, most of the studies presented in the literature focus on steady-state conditions in which lubrication regimes are described using Stribeck curves. Friction evolution is often represented as a function of the Hersey number, i.e., a combination of viscosity, frequency, or relative velocity between contact surfaces and pressure parameters.[1] At relatively low Hersey number (e.g., at low velocity), a sliding lubricated contact works in the boundary regime where asperity contacts occur and the friction value is rather high. At high Hersey number (e.g., at high velocity), a steady full lubricant film completely separates both surfaces and the friction is viscous. At intermediate Hersey number, the regime is defined as mixed. Time-varying conditions, such as accelerations/decelerations, can induce transitions from a hydrodynamic regime to a boundary regime.[2] In sliding oscillating conditions, the friction force displays a hysteretic behavior.[3] Hence, friction-Hersey number curves form cycles and do not comply with a Stribeck curve as classically observed in steady-state conditions.

In parallel, the consideration of steady-state conditions led to broadly used equations of hydrodynamic film characteristics. In the case of elasto-hydrodynamic lubrication (EHL) contacts, the film thickness can be accurately predicted by Hamrock-Dowson or Moes-Venner equations.[4,5] Since the works of Cameron and Gohar,[6,7] these films and their distribution in the contact are also well measured using optical interferometric observations. For time-varying conditions, the lubricated interface can display additional features such as successive squeeze, starvation, and cavitation phenomena.[8] These features depend on parameters such as the velocity or the deceleration rate, for instance. The film thickness prediction requires the resolution of the full Reynolds equation including the transient term, which is much more complex and time-consuming.[9] Usually, the numerical simulation fails to

correctly account for the time effects on the dynamics of the lubricant at the interface. For instance, in sliding oscillating conditions, the film thickness displays a hysteretic behavior as observed for the forces.[10] The squeeze effect causes a lag between the velocity and the film thickness variation during the oscillations.[11]

Various apparatus were developed to measure contact forces under oscillating conditions. Under moderate applied contact pressure (<50 MPa), the friction dynamics of self-assembled monolayers[12] and polymer layers[13] were analysed using the Ecole centrale de Lyon-Surface Force Apparatus (SFA). With this device, simultaneous normal and tangential oscillating displacements at the picometer scale can also be used to get the rheological behavior of confined molecular films.[14,15] The oscillating displacement is performed by piezo-electric translators and the average film thickness is simultaneously measured using capacitive transducers. For high frequency reciprocating motion and higher contact pressure, shaker tribometers are commonly used in the field of fretting sliding (i.e., amplitudes of sliding lower or equal to the contact length) and reciprocal sliding (i.e., amplitudes of sliding generally much larger than the contact size). For instance, Tonck *et al.*[16] developed a reciprocating shaker tribometer to study both Mindlin-type contact and the mechanical behavior of tribochemical films under cyclic tangential load at 80 Hz and amplitudes from 30 to 300 nm. Combining these measurements with post-mortem optical observations, they showed that the tangential stiffness and the tribochemical films wear behavior could not be correlated. More recently, the tribological response of a lubricated interface under free oscillating motion was investigated by Rigaud *et al.*[17] They used a dynamic oscillating tribometer[18] to identify instantaneous velocity-dependent and velocity-independent contributions to friction. Only few tribometers combine friction force measurements with simultaneous interferometry technique to correlate the instantaneous behavior of the film formed at the interface to the friction response (e.g., see Refs. 19 and 20). These works confirm that the knowledge of both film and friction gives new insights into the tribology of lubricated contacts under time-varying conditions by allowing an investigation of the interface at the sub-micrometer scale for few microseconds.

The purpose of this paper is to present a novel instrumented tribometer. The originality of this apparatus is the simultaneous measurement of instantaneous contact forces and *in situ* visualization of the lubricating film distribution under controlled forced oscillating conditions for a large range of amplitudes (5 μm to 2.5 mm) and frequencies (5 Hz to 250 Hz). This tribometer is then used to illustrate the possibilities of measurements for a lubricated contact and the first results are presented.

II. PRESENTATION OF THE CHRONOS TRIBOMETER: MECHANICAL DEVICE AND INSTRUMENTATION

The instrumented forced oscillations tribometer CHRONOS is a reciprocal tribometer configured with a ball-on-flat contact (Fig. 1). The fixed part supports a 25.4 mm steel ball. The transparent moving counterpart is a pellet with

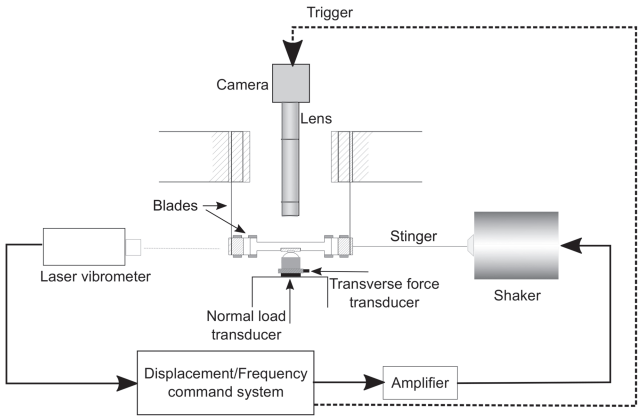

FIG. 1. Instrumented forced oscillations tribometer (CHRONOS).

a diameter of 10 mm and a thickness of 3 mm. For optical measurement of lubricant film thickness, this counterpart is in quartz ($E = 70$ GPa) or sapphire ($E = 400$ GPa) with an additional semi-reflective coating.

Before an experiment, the load is applied from the micrometric vertical displacement of the sphere. The load is accommodated through an elastic deformation of horizontal steel blades fixed on the sample holder. The flat surface oscillating motion is performed by a shaker connected to an active vibration control system to regulate both the sinusoidal motion frequency and amplitude. Displacement and velocity are measured using a Polytec OFV5000 laser vibrometer. In this way, the tribometer can impose a range of strokes between 2.5 mm, much larger than the contact size, and 5 μm, much smaller than the contact size (Fig. 2(a)). Below this value, the system cannot impose an accurate sliding distance. The minimum frequency of oscillating motion is 5 Hz unless the contact reaches seizure conditions. The maximum frequency is the function of the set stroke (Fig. 2(b)). For instance, for a stroke equal to 100 μm, the frequency can reach more than 250 Hz (i.e., a maximum velocity of 350 mm/s at the centre of the stroke). For a stroke of 1 mm, the maximum frequency is 70 Hz (i.e., a maximum velocity of 150 mm/s).

Experiments can be performed under various operating conditions:

- Stroke amplitude and motion frequency are constant;
- The stroke is imposed (e.g., 1 mm) and the motion frequency is linearly swept (e.g., from 50 to 5 Hz);
- The frequency is imposed (e.g., 50 Hz) and the stroke is linearly swept (e.g., from 1 to 0.1 mm);
- The stroke and the frequency are simultaneously and linearly swept (e.g., from 50 Hz to 5 Hz and from 0.1 mm to 1 mm) to keep a constant maximal sliding velocity at the centre of the oscillations.

The normal load is measured using a strain gauge Tei FSB101 normal force transducer (range ±20 N). The friction force is measured using a Kistler 9203 piezoelectric transverse force transducer (range ±500 N). Data are acquired with a four channel cards from National Instruments NI USB-9233.

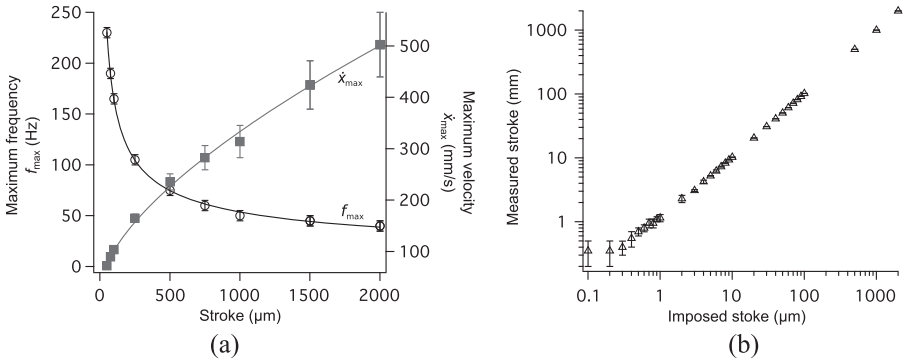

FIG. 2. CHRONOS tribometer operating limits: (a) maximum frequency and velocity as a function of set stroke; (b) measured stroke as a function of the imposed stroke.

The normal load is usually set between 1 N and 20 N. The corresponding mean contact pressure and the contact radius are, respectively, between 200 MPa and 540 MPa and between 40 μm and 110 μm.

An optical system associated with a high speed camera is adapted over the sliding contact to track the lubricant film dynamics. This optical system is an assembly of tubes and lenses allowing a magnification range from 2.5 up to 31. These magnifications, respectively, correspond to a resolution of 2.2 μm/pixel and 0.2 μm/pixel. The lighting system uses an optical fiber fixed on the optical system. A semi-reflecting mirror is contained in the tubes assembly to illuminate the contact. The high speed camera, JAI SP-12000-CXP4, has a maximum resolution of 4096 × 3072 pixels with an associated maximum frame rate of 189 fps. By reducing the region of interest, the maximum frame rate can be substantially increased.

The signals illustrated in the remaining of this paper were acquired with the following experimental conditions:

- A ball-on-flat steel/quartz or steel/sapphire contact lubricated with a 20 μl drop of polyalphaolefin PAO40. The lubricant viscosity is about 706 mPa.s at a room temperature of 23.5 °C and about 826 mPa.s at 20.5 °C.
- The surface roughness of both sphere and flat was measured using a Bruker interferometric profilometer at R_a = 14 ± 1 nm.
- An additional 200 nm silica thick-spacer layer was superimposed on the chromium semi-reflective coating of the flat to measure thin films down to 2 nm.
- A constant normal load of 9.8 ± 0.3 N. Using the quartz flat, this load corresponds to a mean contact pressure of 232 MPa and a contact radius of 116 μm. With the sapphire flat, the mean contact pressure is about 430 MPa and a contact radius of 85 μm.
- A stroke of 1 mm.
- A linear sweep of the oscillating frequency from 50 Hz to 5 Hz with a constant decrement of 0.25 Hz/s. This corresponds to a linear decrease of the maximal sliding velocity at the center of oscillations from 157 to 15.7 mm/s.
- For the lubricant film thickness measurement, the camera was set at 1600 × 500 pixels using a resolution of 1.6 μm/pixel and a frame rate of 1000 fps.

In these conditions, neither wear nor roughness modification was observed after the experiments. Most of the tests were performed at a room temperature of 23.5 °C. Some signals were acquired at a lower room temperature of 20.5 °C. In this case, as the room temperature changes the lubricant viscosity, the lubricant thickness in the contact is different.

III. TIME-FREQUENCY ANALYSIS

A. Time-frequency representations

Figure 3 displays the time evolution of the velocity and the friction coefficient. The friction coefficient is calculated by the ratio of the instantaneous transverse force to the constant normal load. During an experiment, the displacement is sinusoidal with a constant amplitude. This confirms that the active vibration control system allows a sinusoidal displacement with a constant amplitude. The velocity is sinusoidal with a phase shift of $\frac{\pi}{2}$ relative to the displacement and a linear decreasing amplitude according to the frequency. During an oscillation period, the velocity is maximal at the middle of a stroke and null at the edges of a stroke. In parallel, the friction coefficient is neither in phase with the displacement nor with the velocity. The friction coefficient exhibits a different shape according to the frequency but remains periodical. It displays a main periodicity corresponding to the harmonic excitation frequency (i.e., the imposed oscillating frequency). Secondary periodicities corresponding to additional harmonic frequencies are also contained within the temporal signal. These harmonic periodicities are observed at high frequency and vanish at low frequency.

The spectrograms of the displacement and the friction highlight these harmonics in the signals (Fig. 4). The shaker generates a displacement with the decreasing frequency from 50 Hz to 5 Hz clearly represented by an intense excitation frequency signal on the spectrogram (Fig. 4(a)). Additional and less intense harmonics are also visible on the spectrogram. Consequently, the contact reacts not only to the excitation frequency but also to these harmonics (Fig. 4(b)). The friction amplitude decreases along the other harmonic orders. In addition, the spectrogram in Figure 4(b) shows device frequency modes between 200 Hz and 300 Hz. These modes slightly interfere with the friction signal. Therefore, a band-stop filter is applied at 220 Hz to remove these interferences in the friction signal.

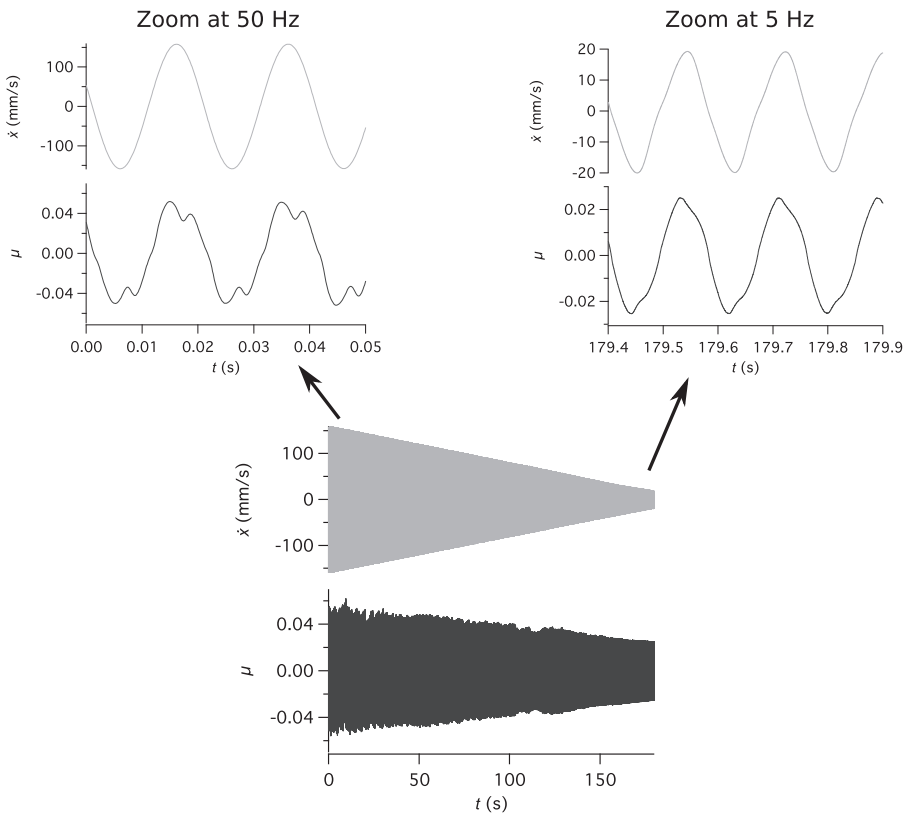

FIG. 3. Velocity and friction coefficient synchronized temporal signals from 50 Hz to 5 Hz.

B. Logs and cycles

In a log representation, the friction vs. displacement curve goes from wavy cycles at high frequencies to a more elliptic form at low frequencies (Fig. 5(a)). Again, this expresses that the response to the harmonic frequencies tends to vanish towards the low frequencies. The friction vs. velocity also goes from wavy cycles at high frequencies to smooth cycles at low frequencies (Fig. 5(b)).

Cycle representations give a clearer view of the friction variations. For a constant stroke of 1 mm, the friction vs. displacement cycles show that friction amplitude decreases with the sliding frequency (Fig. 6(a)). The friction vs. velocity cycles become thinner as the sliding frequency decreases (Fig. 6(b)). Indeed, at lower frequencies, the film thickness is more likely to follow the changes in velocity without hysteresis. The angle of the cycles with the horizontal axis increases with the decreasing frequency. The tilt angle may be related to a lower dependence of friction with the velocity when the sliding frequency is low. This evolution could not be linked to wear or to a roughness modification during or after the experiments. These signals are a dynamic signature of complex processes occurring in the oscillating lubricated interface.

C. Calculated parameters

A complementary approach consists of looking at averaged phenomena. The following four parameters are systematically calculated through moving averages using a

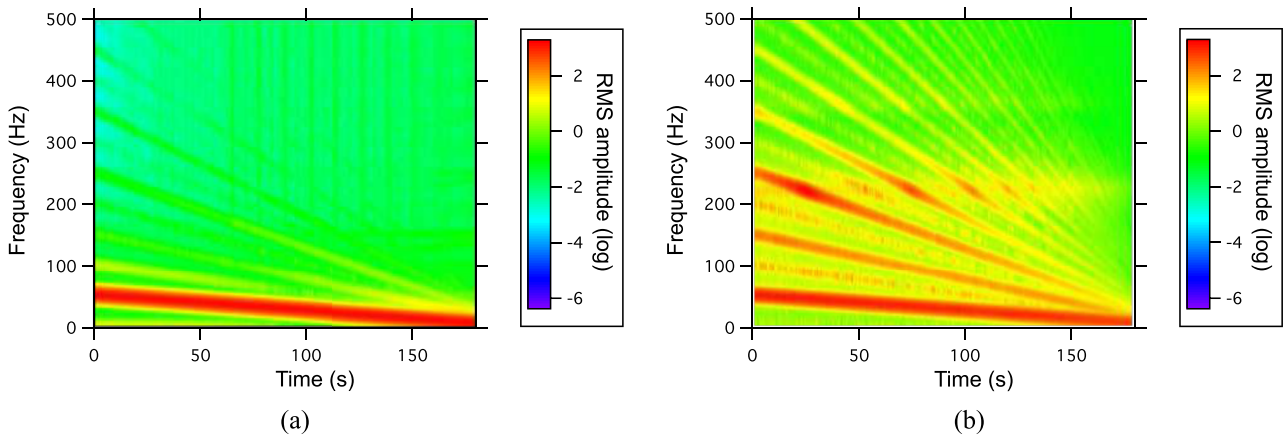

FIG. 4. Time-frequency analysis: (a) Displacement spectrogram; (b) friction coefficient spectrogram.

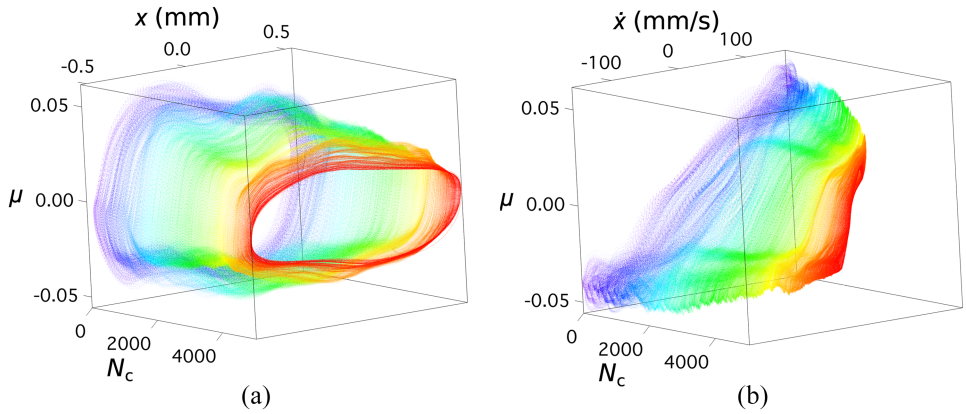

FIG. 5. Log representations of friction considering the number of cycles N_c (rainbow color from purple-blue at 50 Hz to red at 5 Hz): (a) as a function of the displacement x; (b) as a function of the velocity $\dot{x}$.

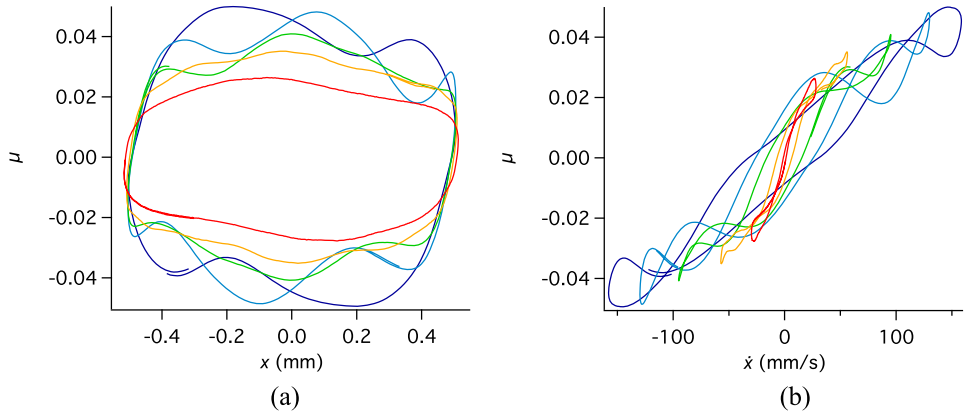

FIG. 6. Friction instantaneous cycles at 48, 39, 27, 16, and 7 Hz from purple-blue to red: (a) as a function of the displacement x; (b) as a function of the velocity $\dot{x}$.

convolution product with a n-dimension rectangular function $\prod(t)$ (n is the sampling size) (Eq. (1)):

- The friction coefficient moving average $\langle\mu(t)\rangle$ (Eq. (2)).
- The velocity moving average $\langle\dot{x}(t)\rangle$ (Eq. (3)).
- The dissipated energy at the interface moving average $\langle E_d(t)\rangle$ (Eq. (4)).
- The $\mu(\dot{x})$ cycles average tilt $\theta(t)$ (Eq. (5)).

$$\prod(t) = \begin{cases} 1/n, & \text{if } t < n \\ 0, & \text{if } t > n \end{cases}, \tag{1}$$

$$\langle\mu(t)\rangle = \sqrt{\prod(t) * \mu^2(t)}, \tag{2}$$

$$\langle\dot{x}(t)\rangle = \sqrt{\prod(t) * \dot{x}^2(t)}, \tag{3}$$

$$\langle E_d(t)\rangle = \sqrt{\prod(t) * [F_T(t) \cdot x(t)]^2}, \tag{4}$$

$$\theta(t) = \arctan\left[\frac{\langle\mu(t)\rangle}{\langle\dot{x}(t)\rangle}\right]. \tag{5}$$

The $\langle\mu(t)\rangle$ vs. $\langle\dot{x}(t)\rangle$ is used to make analogies with the steady-state conditions as shown in Figure 7. Here, the averaged friction coefficient is below 0.05 and slightly rises as the velocity increases. This suggests that the contact works in a full-film lubrication regime in which the friction force has a purely viscous origin. The averaged dissipated energy curve is similar in variation to the averaged friction coefficient as the strokes are constant. The cycles average tilt decreases with the averaged velocity.

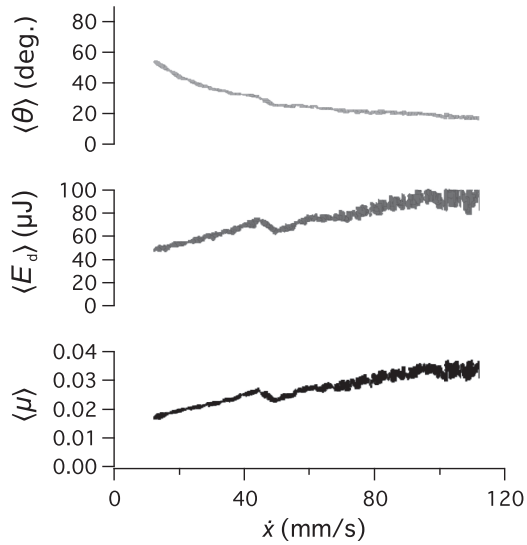

FIG. 7. Averaged parameters of the sliding contact as a function of the velocity moving average (friction-velocity cycles tilt angle and average signals of dissipated energy and friction coefficient).

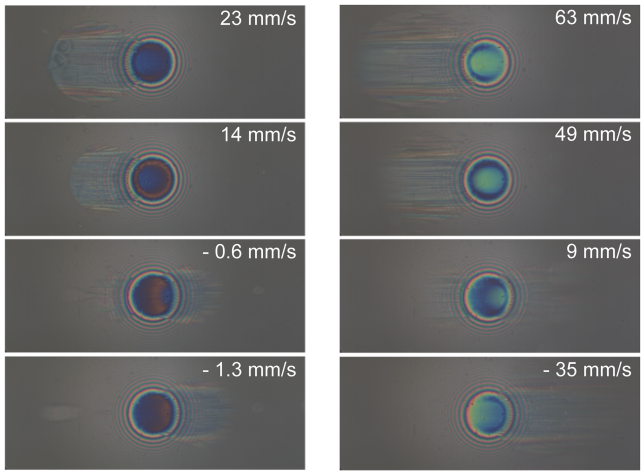

FIG. 8. Interferometric images of the lubricated sliding contact (radius of 86 μm) extracted from videos with a frame rate of 180 fps (the velocity is positive for the lubricant flow direction from the right to the left): (a) sliding frequency of 6 Hz; (b) sliding frequency of 20 Hz.

IV. CONTACT IMAGE ANALYSIS

A. Contact observations

In the nominal conditions and at a room temperature of 23.5 °C, Figure 8 illustrates the contact interferograms obtained at 6 Hz (a) and 20 Hz (b) at various instants during oscillations. At 23 mm/s (Fig. 8(a)), the contact is in full-film regime with a homogeneous separation of the surfaces in the contact centre (blue colored area) and the classical horseshoe shape constriction zone.[1] The fluid flows from right to left. As the velocity decreases, the constriction extends towards the contact entrance at the right of the interferogram. A strongly heterogeneous film distribution can be seen at −0.6 mm/s where the central dimple of fluid is entrained towards the outlet zone. The fluid now flows from left to right. Red/orange colors are the representative of the thinnest lubricant films. Thicker lubricant films are displayed in blue/green colors (Fig. 8(b)). Classically, the lubricant film thickness in the contact centre increases with the velocity as shown by the comparison between interferograms at 23 mm/s and 63 mm/s.

B. Film thickness measurements

A program was built on Igor pro software to automatically measure the lubricant film thickness distribution in the contact with the acquired video sequences. To do this, the program correlates the interferometric colors of the interface during experiments with the static calibration images. As described in various studies,[21] this correlation is made by minimizing the Euclidian distance among RGB (Red Green Blue), HSL (Hue Saturation Lightness), and/or Lab (Lightness and color-opponent dimensions) color components. With this program, a great number of longitudinal lubricant thickness profiles can be plotted during the experiments.

In the experimental conditions described above, during an acceleration, the lubricant film thickness profiles continuously go from a trapezoidal form to the classical profile observed during steady-state EHL conditions (i.e., a constriction zone and a central flat zone are observed) (Fig. 9(a)). During a deceleration, the lubricant film thickness profiles go from a classical profile to profiles displaying a central lubricant constriction zone (Fig. 9(b)). Finally, as shown at the end of the deceleration, the lubricant flows out of the contact. The dissymmetry of the lubricant film thickness distribution between the acceleration and the deceleration periods has to be related to the hysteresis observed in the $\mu(x)$ cycles and its evolution with time.[22]

The representation of synchronized curves of velocity $\dot{x}$, friction coefficient μ, and central film thickness h_c gives additional information on the interface mechanisms (Fig. 10). For instance, at an oscillation frequency of 20 Hz and at a room temperature of 20.5 °C, the central lubricant film thickness is periodical and the periodicity T is similar to the velocity's. Subsidiarily, as the room temperature is lower here than for the measurement realized for Figure 9, the central lubricant film is thicker. At the beginning of a stroke, during accelerations, h_c drops then increases with a lag according to the velocity. During the acceleration, a local drop of central film thickness may occur probably because of dynamic phenomena in the inlet. At the middle of a stroke, h_c reaches a plateau before the next stroke and a new drop of film thickness. Here, the friction coefficient mainly follows the velocity variations and appears to be modulated by the lubricant film thickness.

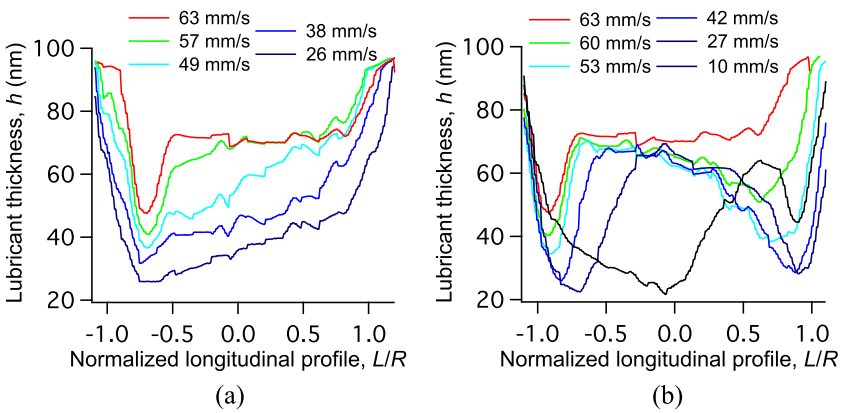

FIG. 9. Lubricant film thickness longitudinal profiles over one stroke measured at an oscillation frequency of 20 Hz (with L/R the ratio between the longitudinal distance on the contact radius): (a) during an acceleration from 0 to 62 mm/s; (b) during a deceleration from 62 mm/s to 0.

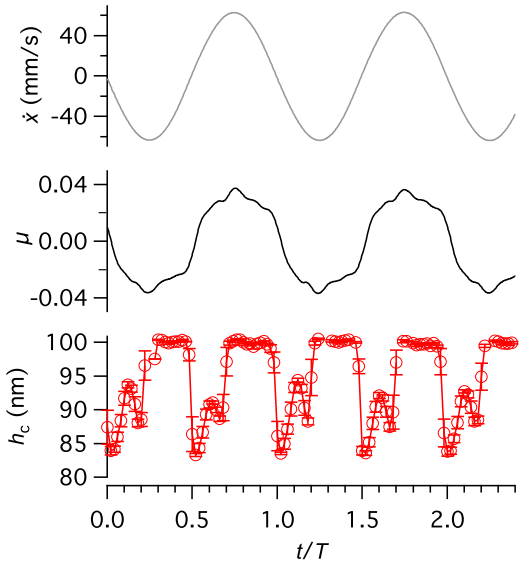

FIG. 10. Superimposition of the velocity $\dot{x}$, the friction coefficient μ, and the central lubricant film thickness h_c measured at an oscillation frequency of 20 Hz.

V. DISCUSSION AND PROSPECTS

The CHRONOS apparatus can detect subtle friction modifications of the oscillating lubricated interface. This device can set up a reciprocating sliding contact with a micrometric resolution in displacement and a large range of frequencies up to 250 Hz. The first experiments showed that the friction exhibits a hysteretic behavior with motion. The squeeze effect combined with the lubricant flow in and out of the contact is likely at the root of this phenomenon. Different approaches of signal processing and graphical representation as logs, cycles, and moving averages can provide a better description of the friction behavior.

The consideration of moving averages, as $\langle\mu(t)\rangle$ vs. $\langle\dot{x}(t)\rangle$, can be a way to analyse the transient lubrication process. The dissipated energy will bring additional information on the friction behavior with variable strokes. The cycle average tilt is another interesting parameter which can lead to a mean lubrication regime identification by expressing the velocity-dependence of friction.

The simultaneous interferometric measurement of film thickness distribution with a speed camera should confirm or infirm these approaches. For instance, in this preliminary study, the low averaged friction indicates a full film lubrication mechanism and indeed the lubricant thickness is always above 20 nm. This may explain that here $\langle\mu(t)\rangle$ increases with $\langle\dot{x}(t)\rangle$ which is characteristic of a viscous regime usually observed when the surfaces are fully separated by the lubricant film. The lubricant thickness never reaches zero even when the oscillating velocity crosses zero. This is the result of the lubricant dimple formed during the squeeze.

In the very near future, the CHRONOS tribometer will allow us to investigate lubricated contact dynamic behavior. This tribometer opens a new field of research and understanding of the role of experimental conditions, such as velocity, contact pressure, stroke distance, and the inlet lubricant volume, on the lubrication mechanisms under oscillating conditions. The lubricant properties are another way of investigation. Finally, the surface properties are also a point of interest by focusing on the surface roughness and on the presence of adsorbed layers.

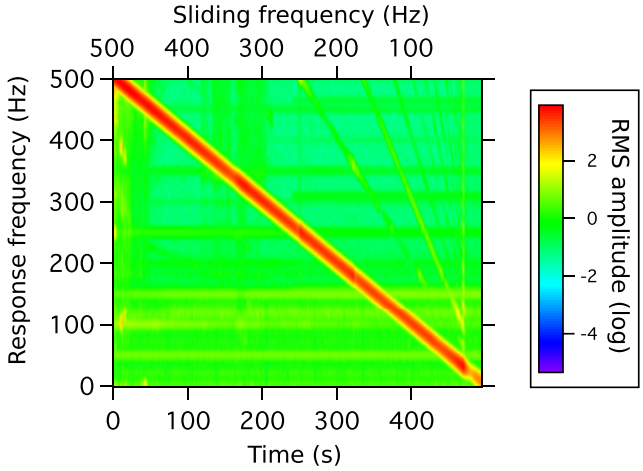

FIG. 11. Transverse force spectrogram in dry friction.

ACKNOWLEDGMENTS

This work was funded by the French Agence Nationale de la Recherche under the Confluence Project No. ANR-13-JS09-0016-01.

APPENDIX: TRANSVERSE FORCE SPECTROGRAM

To characterize the device transverse force measurement, a complementary experiment was performed in dry friction. The contact was set with a stroke of 10 μm and a load of 5 N. A linear sweep of the oscillating frequency was performed from 500 Hz to 5 Hz with a constant decrement of 1 Hz/s. The spectrogram of the measured transverse force shows an intense response along the excitation frequencies (Fig. 11). Neither intense additional frequency mode nor harmonic is observed here.

[1] B. J. Hamrock, S. R. Schmid, and B. O. Jacobson, *Fundamentals of Fluid Film Lubrication* (Marcel Dekker, 2004).
[2] A. Ernesto, D. Mazuyer, and J. Cayer-Barrioz, "From full-film lubrication to boundary regime in transient kinematics," Tribol. Lett. **59**(1), 23 (2015).
[3] R. Bassani, E. Ciulli, M. Carli, and K. Stadler, "Experimental investigation of transient and thermal effects on lubricated non-conformal contacts," Tribotest **13**, 183–194 (2007).
[4] B. J. Hamrock and D. Dowson, "Isothermal elastohydrodynamic lubrication of point contacts: Part III - fully flooded results," J. Lubr. Technol. **99**, 264 (1977).
[5] G. Nijenbanning, C. H. Venner, and H. Moes, "Film thickness in elastohydrodynamically lubricated elliptic contacts," Wear **176**, 217–229 (1994).
[6] A. Cameron and R. Gohar, "Theoretical and experimental studies of the oil film in lubricated point contact," Proc. R. Soc. A **291**(1427), 520–536 (1966).
[7] M. Diew, A. Ernesto, J. Cayer-Barrioz, and D. Mazuyer, "Stribeck and traction curves under moderate contact pressure: From friction to interfacial rheology," Tribol. Lett. **57**(1), 8 (2015).
[8] E. Ciulli, "Non-steady state non-conformal contacts: Friction and film thickness studies," Meccanica **44**, 409–425 (2009).
[9] J. Sugimura and H. A. Spikes, "Technique for measuring EHD film thickness in non steady-state contact conditions," in *Elastohydrodynamics*, edited by D. Dowson *et al.* (Elsevier Science B.V., 1997), pp. 91–100.

[10]H. L. Costa and I. M. Hutchings, "Hydrodynamic lubrication of textured steel surfaces under reciprocating sliding conditions," Tribol. Int. **40**, 1227–1238 (2007).
[11]D. P. Hess and A. Soom, "Friction at a lubricated line contact operating at oscillating sliding velocities," J. Tribol. **112**, 147–152 (1990).
[12]D. Mazuyer, J. Cayer-Barrioz, A. Tonck, and F. Jarnias, "Friction dynamics of confined weakly adhering boundary layers," Langmuir **24**, 3857–3866 (2008).
[13]J. Cayer-Barrioz, D. Mazuyer, A. Tonck, and E. Yamaguchi, "Frictional rheology of a confined adsorbed polymer layer," Langmuir **25**(18), 10802–10810 (2009).
[14]A. Tonck, S. Bec, D. Mazuyer, J.-M. Geoges, and A. A. Lubrecht, "The Ecole Centrale de Lyon surface force apparatus: An application overview," Proc. Inst. Mech. Eng., Part J **213**, 353–361 (1999).
[15]D. Mazuyer, A. Tonck, and J. Cayer-Barrioz, "Friction control at the molecular level: From superlubricity to stick-slip," Superlubricity **2007**, 397.
[16]A. Tonck, P. Kapsa, and J. Sabot, "Mechanical behavior of tribochemical film under a cyclic tangential load in a ball-flat contact," J. Tribol. **108**, 117–122 (1986).
[17]E. Rigaud, D. Mazuyer, and J. Cayer-Barrioz, "Interfacial friction law for a circular EHL contact under free sliding oscillating motion," Tribol. Lett. **51**, 419–430 (2013).
[18]E. Rigaud, J. Perret-Liaudet, M. Belin, L. Joly-Pottuz, and J.-M. Martin, "An original dynamic tribotest to discriminate friction and viscous damping," Tribol. Int. **43**, 320–329 (2010).
[19]A. Ernesto, D. Mazuyer, and J. Cayer-Barrioz, "The combined role of soot aggregation and surface effect on the friction of a lubricated contact," Tribol. Lett. **55**, 329–341 (2014).
[20]V. Chauveau, D. Mazuyer, F. Dassenoy, and J. Cayer-Barrioz, "*In situ* film-forming and friction-reduction mechanisms for carbon-nanotube dispersions in lubrication," Tribol. Lett. **47**, 467–480 (2012).
[21]J. Molimard, M. Querry, P. Vergne, I. Krupka, and M. Hartl, "Calculation of pressure distribution in EHD point contacts from experimentally determinated film thickness," Tribol. Int. **38**, 391–401 (2005).
[22]D. Mazuyer, A. Ernesto, and J. Cayer-Barrioz, "Theoretical modelling of film-forming mechanisms under transient Conditions: Application to deceleration and experimental validation," Tribology Letters **65**, 22 (2017).